International Journal of Offshore and Polar Engineering (ISSN 1053-5381)
Copyright © by The International Society of Offshore and Polar Engineers
Vol. 23, No. 1, March 2013, pp. 46–54

http://www.isope.org/publications

Numerical and Experimental Modeling of Regular Wave Interacting with Composite Breakwater

E. Didier
LNEC (Laboratório Nacional de Engenharia Civil)/DHA/NPE, Lisboa, Portugal
MARETEC (Marine and Environmental Technology Center), Instituto Superior Técnico, Universidade Técnica de Lisboa, Portugal

R. Martins and M. G. Neves
LNEC (Laboratório Nacional de Engenharia Civil)/DHA/NPE, Lisboa, Portugal

Numerical modeling of the interaction between waves and coastal structures is a challenge due to the many nonlinear phenomena involved, such as wave propagation, wave transformation with water depth, interaction between incident and reflected waves, runup/rundown and wave overtopping. For simulating such complex free-surface flows, numerical models based on Lagrangian formulation, such as Smoothed Particle Hydrodynamics (SPH), are on option. Even though validation of these numerical models is essential, comparing numerical results with experimental data is not an easy task. In the present paper, an SPH numerical model is validated comparing numerical results of waves interacting with a composite breakwater with data obtained from physical model tests carried out in one of the LNEC's flumes. To achieve this validation, the experimental setup was determined to be compatible with the characteristics and capabilities of the numerical model. Therefore, the flume dimensions are exactly the same for both the numerical and physical model and conditions of wave generation are identical, which allows determining the accuracy of the numerical model, particularly regarding complex phenomena such as wave propagation, wave-breaking and impact loads on the vertical front of the composite breakwater. The numerical results agree well with the physical model tests. The free-surface level is well estimated, with a concordance index between 90% and 97%. Pressure at the vertical wall shows impact loads with high intensity and short duration with a concordance index between numerical and experimental of about 80%.

INTRODUCTION

Coastal structures are built to act as an obstacle to natural wave propagation, creating areas of reduced wave activity. Their efficiency depends on their ability to dissipate or reflect wave energy. Composite breakwaters, consisting of a rubble foundation and a concrete caisson, have been designed as an alternative to rubble-mound breakwaters, with the main advantage of reducing costs, improving hydraulic performance and construction time. However, wave reflection, and especially wave loads, increase considerably due to the characteristics of the cross-section of the composite breakwater.

Prediction of wave forces on caisson-type breakwaters is difficult, especially in the case of impact loads that strongly depend on wave reflection and breaking, which affect wave characteristics near the structure. The forces on a composite breakwater are usually predicted using a semi-empirical formula. However, direct application of this formula is limited to simple structural configurations and to specific wave conditions. In practical engineering case studies, physical modeling is usually also undertaken, which permits a reliable evaluation of the structure's efficiency.

Numerical models have been further developed and their use is becoming increasingly attractive. However, only few numerical models allow the simulation of the complex phenomena of wave breaking and overtopping and forces at vertical structures.

Received June 25, 2012; revised manuscript received by the editors November 22, 2012. The original version was submitted directly to the Journal.

KEY WORDS: Smoothed Particle Hydrodynamics (SPH), wave-structure interaction, coastal engineering, impact loads, physical modeling.

Recently, models based on the Lagrangian method, such as the Smoothed Particle Hydrodynamics (SPH) approach, have emerged. The method is based on the SPH formulation of Navier-Stokes equations and on a completely mesh-free technique. Monaghan, in 1994, showed that SPH is a promising alternative to simulate free-surface flows and wave breaking. Different models have been developed and there are many different numerical implementations. However, there are 2 main numerical approaches for modeling free-surface flows: The weakly-compressible SPH approach (WCSPH), where fluid pressure is related to particle density using an equation of state (Monaghan, 1992; Dalrymple et al., 2001; Crespo, 2008), and the incompressible SPH approach (ISPH), where fluid pressure is calculated solving a Poisson equation (Gotoh et al., 2001; Shao, 2010).

While the kinematics of SPH simulations is generally realistic, the pressure of the particles can exhibit large oscillations. Gómez-Gesteira et al. (2010) show that filtering density (i.e. renormalization of particle density) is necessary to obtain a good representation of a dam-break flow and pressure field without oscillations. However, filtering density influence seems to be more complex for wave propagation.

Recent studies for analyzing the influence of filtering density used in WCSPH models and conventional and Riemann solver-based formulations were performed by Hughes et al. (2010) and Rogers et al. (2010), for regular wave impacting a vertical wall. Hughes et al. (2010) compared ISPH and WCSPH models, with and without filtering density, for waves impacting a vertical wall. Both methods have shown they are able of simulating pressure on the vertical wall due to wave impacts. The predictions for the wave impacts have shown to be in agreement, qualitative and quantitative, with available experimental data. Results from

the WCSPH appear to be significantly smoother than those from ISPH. This is particularly the case for free-surface deformation and especially for wave-breaking. Rogers et al. (2010) simulated forces on a caisson breakwater under the action of waves impinging on the vertical wall of the structure. The WCSPH Riemann solver-based formulation implemented in the SPHysics model (Gómez-Gesteira et al., 2010) is used, and it showed that results are in better agreement with experimental data than those obtained using the conventional filtering WCSPH SPHysics formulation (Gómez-Gesteira et al., 2008). However, no sensitivity study was made with particle dimension even thought it was pointed out that this is a crucial issue for model accuracy. Didier et al. (2011) and Martins (2012) showed that conventionally used, total filtering density stabilizes the pressure field but causes a numerical diffusion on wave propagation and a consequent reduction on wave height not observed in the experimental results. On the other hand, without filtering density, unphysical pressure oscillations occur and forces on structures cannot be calculated. So, a partial filtering density technique, i.e. renormalization applied only for particles near the structure, is developed and seems to be a promising compromise that allows simultaneously propagating waves, without diffusion, and accurately modeling the pressure field near the structure, without oscillations.

The WCSPH model under development at the National Civil Engineering Laboratory (LNEC) is based on the original SPHysics model (Gómez-Gesteira et al., 2008; SPHysics code, version 1.4, 2008) inspired by the formulation of Monaghan (1992); it has been especially developed for studies of wave interacting with coastal structures. Promising agreement with experimental data has been obtained for both free-surface elevation and overtopping discharge for impermeable coastal structures (Didier et al., 2009a, b; 2010a, b). However, the validation has been made with results from physical model tests not specifically designed for model validation and with an experimental setup that differ from the numerical model's one.

The paper presents the validation of WCSPH numerical model to the study of waves interacting with a composite vertical breakwater. To achieve that goal, a set of physical model tests was performed at LNEC in a wave flume with the experimental setup and boundary conditions compatible with the numerical model characteristics. Therefore, the flume dimensions and the piston-type wave-maker movement are the same for both numerical and physical models, which allows determining the accuracy of the numerical model, particularly regarding 2 complex phenomena: wave propagation and wave impacts on the composite vertical breakwater.

SPH NUMERICAL MODEL

The 2D momentum conservation equation and the conservation law, in Lagrangian form, for a viscous fluid are written as:

$$\frac{dv}{dt} = -\frac{1}{\rho}\nabla P + \Pi + g \tag{1}$$

$$\frac{1}{\rho}\frac{d\rho}{dt} = -\text{div}\,(v) \tag{2}$$

where v refers to the velocity, P the pressure, ρ the fluid density, Π the diffusion terms, and $g = (0, -9.81\ \text{m/s}^2)$ the gravitational acceleration.

The actual SPH model used and underdeveloped at LNEC is based on the SPHysics code (Crespo et al., 2008a, b; Gómez-Gesteira et al., 2008, 2010), version 1.4 (SPHysics code, version 1.4, 2008). As noted above, the weakly-compressible SPH numerical approach, based on the standard SPH formulation of Monaghan (1992), is used.

For numerical simulations of wave propagation, the quadratic kernel (Johnson et al., 1996; Dalrymple and Rogers, 2006) is used to determine the interaction between the particles.

The Sub-Particle Scale (SPS) laminar viscosity turbulence model (Gotoh et al., 2001; Rogers and Dalrymple, 2004) is used because it includes not only a model of laminar viscosity but also the effects related to the turbulence through a model derived from the Large Eddy Simulation. It also provides better results when compared to the artificial viscosity model, since the SPS model avoids the strong dissipative effects of the artificial viscosity model (Didier and Neves, 2009b).

Fluid particles are usually moved using the XSPH correction method (Monaghan, 1989), which consists of a correction for the particle velocity. However, Didier and Neves (2009b) have shown that instabilities appear during wave propagation and particles cross the solid boundary when this correction is used. Consequently, the XSPH correction is not used here for wave propagation.

The fluid is treated as weakly compressible, which allows using the equation of state (Batchelor, 1974) relating pressure with density. A partial filter density technique is applied for simultaneously propagating waves and modeling accurately the pressure field near the structure (Didier et al., 2011; Martins, 2012).

Numerical integration in time is performed by the Predictor-Corrector model using a variable time step to ensure the CFL condition.

The repulsive boundary condition developed by Monaghan and Kos (1999) is used and prevents particles crossing a solid boundary.

Initially, the water particles are placed in the flume using a uniform Cartesian grid, with spacing between particles defined by *do*. Velocity is zero and pressure is hydrostatic.

The wave paddle movement in the numerical simulations is the same as used for physical tests where dynamic absorption is not used.

Details of numerical implementation are available in Gómez-Gesteira et al., 2008; SPHysics code version 1.4, 2008; and Didier and Neves, 2012.

PHYSICAL MODELING OF WAVE INTERACTING WITH COMPOSITE BREAKWATER

Within the objective of validating the SPH numerical model, physical model tests of several coastal structures are performed in one of the LNEC's flumes, 49.4 m in length, 1.6 m in width, 1.2 m in height. The flume is equipped with a piston-type wave-maker and generates both regular and irregular waves.

The physical model setup was determined in such a way that the exact replication in the numerical model was feasible, taking into account the limitations of the numerical model dimensions and of the CPU time due to numerical resolution, as well as the wave generation conditions. So, numerical and experimental conditions are identical.

The coastal structure consists of an impermeable composite breakwater composed by a berm, 0.181 m in height and with a 1:3 slope, and an 0.03-m-thick acrylic vertical wall reinforced by vertical supports on its rear part to ensure rigidity of the structure, located 0.2 m from the top of the slope (Fig. 1). The crest freeboard is 0.3 m above the water level. The horizontal bottom between the piston-type wave-maker and the beginning of the 1:3 slope is 3.62 m long.

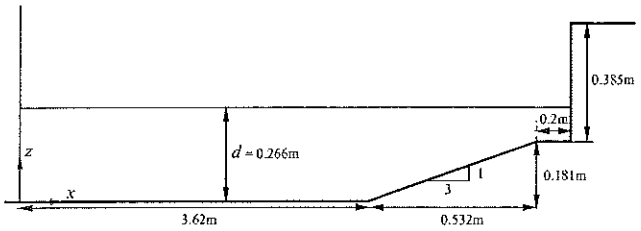

Fig. 1 Schematic representation of wave flume and structure, coordinate system and dimensions

Regular waves were tested with 2 wave periods, T, of 1.1 s and 1.3 s, and wave heights, H, varying from 0.04 m to 0.16 m. Two water depths, d, were tested, 0.325 m and 0.266 m, which result in wave lengths L, 2.02 m and 1.51 m (Martins, 2012). The tests lasted long enough to generate at least 10 regular waves. Active absorption of the reflected waves at the wave-maker was not used in the present tests.

For the conducted tests, experimental data were collected in 2 resistive-type wave gauges (developed at LNEC) and 6 pressure sensors (model AB/HP pressure transducers with a diaphragm size of 19 mm and maximum pressure 20000 PSI, from Honeywell). The first gauge (G1), located 2.643 m from the wave-maker's initial position, $x = 2.643$ m, was placed to verify the generated wave characteristics; the second gauge (G2), located on the slope at $x = 3.943$ m, to verify wave conditions near the structure. The pressure sensors were located at the front face of the vertical wall, approximately in the middle of the wall to limit the effects of the flume walls. The center of pressure sensor P1 is located 0.055 m above the berm. The center of sensor P2 is placed 0.055 m above the center of P1, the center of P3 0.055 m above the center of P2, etc. Fig. 2 shows the wave flume with the composite breakwater and the position of the sensors.

A frequency of 400 Hz was used for data acquisition in both wave gauges and pressure sensors due to the available equipment. Usually, to measure impact pressure a sampling rate greater than 1 kHz is recommended.

Each wave condition was repeated 10 times. For all wave conditions and water levels, test repetitions present a good agreement: for $d = 0.266$ m, $T = 1.3$ s and wave heights from 0.04 m to 0.14 m, the maximum deviation between test repetitions, before wave re-reflection on the wave-maker, is ± 0.005 m. After re-reflection on the wave-maker, differences on the free-surface level are slightly larger.

For analyzing quantitatively the deviation of repetitions, i.e. the precision of measurements, the mean free-surface elevation at gauges G1 and G2 and pressure at pressure sensor P1 are calculated from each repetition. The minimum and maximum deviation and the root mean square (RMS) are calculated along the time

Fig. 2 Composite breakwater at flume with pressure sensors at front face

	RMS		
H (m)	G1 (m)	G2 (m)	P1 (m H_2O)
0.04	5.43×10^{-3}	9.84×10^{-3}	2.90×10^{-2}
0.06	4.91×10^{-3}	1.12×10^{-2}	1.17×10^{-1}
0.08	8.37×10^{-3}	8.81×10^{-3}	1.52×10^{-1}
0.10	8.38×10^{-3}	1.13×10^{-2}	1.65×10^{-1}
0.12	8.00×10^{-3}	1.10×10^{-2}	1.60×10^{-1}
0.14	1.58×10^{-2}	1.43×10^{-2}	1.43×10^{-1}
0.16	1.57×10^{-2}	1.50×10^{-2}	1.47×10^{-1}

Table 1 Root mean square of free-surface elevation at gauges G1 and G2 and of pressure at sensor P1 ($T = 1.3$ s, $d = 0.266$ m)

series, for each acquisition point. The maximum RMS is also calculated and shown Table 1. It can be seen that the maximum RMS of the free-surface elevation remains small and has varied from 4.91×10^{-3} m to 1.58×10^{-2} m for the smaller and higher wave height, respectively. Maximum RMS is larger on gauge G2 than G1 due to the variability of wave-breaking and wave-reflection characteristics along the 10 repetitions. As noted above, differences in free-surface elevation are slightly larger after re-reflection on the wave–maker.

Fig. 3 shows the mean and the RMS of free-surface elevation measured at gauges G1 and G2 for an incident wave height $H = 0.10$ m. The RMS is larger for gauge G2 than for G1. The deviation increases with time as the effect of re-reflection on the free-surface elevation along the flume increases. However, analyzing the maximum variation (RMS) of free-surface elevation at the 2 gauges, it is less than ± 0.007 m and ± 0.015 m respectively for G1 and G2.

Overall pressure deviation shows also a good agreement despite its higher RMS values, ranging from 2.90×10^{-2} m H_2O to 1.65×10^{-1} m H_2O (Table 1). The phenomena involved and the high turbulent nature of the flow combined with the very short duration of the pressure peaks and the variability of the impact point, which are difficult to capture, are some of the possible reasons for these higher values. Fig. 4 shows the mean and RMS pressure at sensor P1 for an incident wave height of 0.10 m. It can be seen that maximum deviation occurs at the impact. It can be noted that no filter is used in the time series of pressure.

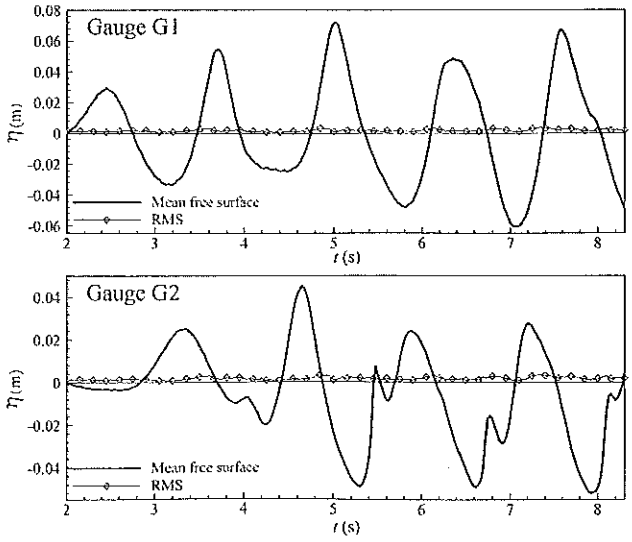

Fig. 3 Mean and RMS of free-surface elevation at gauges G1 and G2 ($T = 1.3$ s, $H = 0.10$ m, $d = 0.266$ m)

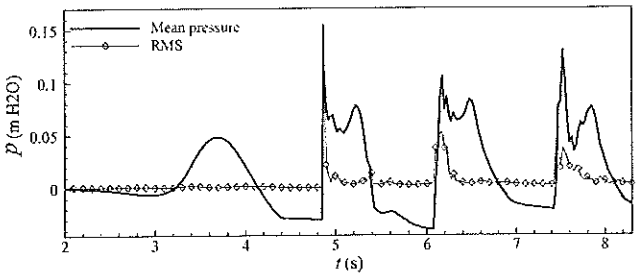

Fig. 4 Mean and RMS pressure at sensor P1 ($T = 1.3$ s, $H = 0.10$ m, $d = 0.266$ m)

RESULTS AND DISCUSSION

In the present study, numerical simulations are performed for the same wave period and water depth ($T = 1.3$ s and $d = 0.266$ m) and for wave heights, $H = 0.04$, 0.06, 0.08, 0.10, 0.12, 0.14 and 0.16 m. Simulations are carried out using a resolution with $do = 2.66$ mm, that corresponds to a particle volume equal to 7.076×10^{-6} m^3/m. The number of fluid and solid particles used for the present simulations is 155612. The mean time step is around 2.4×10^{-5} s. Computational time is 83 h for modeling 9 s, using a serial version of the code and a Personal Computer Intel(R) Core(TM) i7 CPU 930 @ 2.80 GHz.

As indicated below, a partial filtering density technique is implemented in the SPH code. Fig. 5 shows the free-surface elevation at gauges G1 and G2 for $H = 0.12$ m and 3 density filters, for a resolution with 125920 particles: without re-normalization, total re-normalization (i.e. filter applied for all particles) and partial re-normalization (i.e. filter applied only for particle from $x = 4.06$ m to the end of the flume). Without filtering density, unphysical pressure oscillations occur and forces on structures cannot be calculated. On the other hand, conventional use of total re-normalization causes a numerical diffusion on wave propagation and a consequent reduction on wave height, but stabilizes the pressure field. The partial filtering density technique allows simultaneously propagating waves, without diffusion, and the more accurate modeling of the pressure field near the structure, without large oscillations.

A sensitivity study with particle dimension is a crucial issue for model accuracy, as noted above. For this case study, convergence of results with particle dimensions, *do*, was analyzed for 4

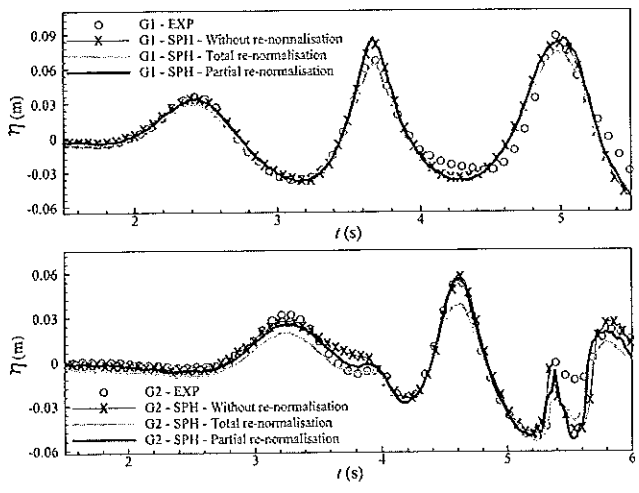

Fig. 5 Free-surface elevation (gauges G1 and G2) for 3 types of filter density, $H = 0.12$ m

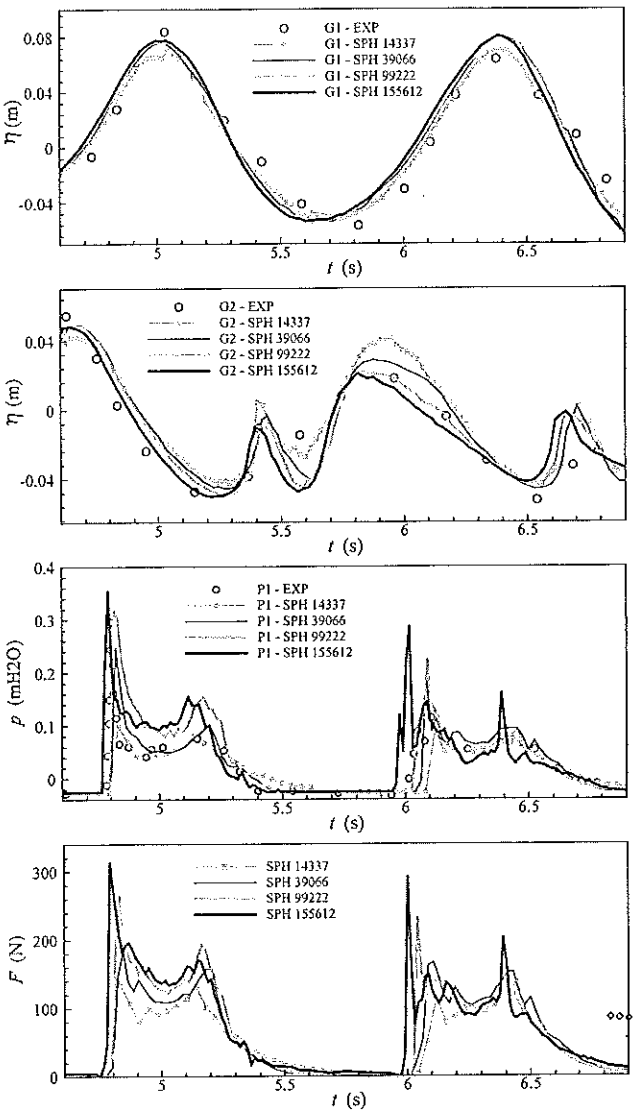

Fig. 6 Free-surface elevation (gauges G1 and G2), pressure (sensor P1) and force on vertical wall, F, for 4 resolutions, $H = 0.12$ m

resolutions with *do* equal to 8.87, 5.32, 3.32 and 2.66 mm (i.e. a number of particles, N, 14337, 39066, 99222 and 155612) for an incident wave with $T = 1.3$ s and $H = 0.12$ m on a depth $d = 0.266$ m. Fig. 6 presents SPH results for 4 resolutions together with experimental data. The results showed that, at gauge G1, convergence on the free-surface elevation is obtained from medium resolution ($N = 39066$). However, at G2, where the breaking and reflection affect the shape of the wave, the convergence is not so clear, even though convergence seems to be obtained for the finer resolutions, $N = 99222$ and 155612. Particle mass increases when resolution is coarser, resulting in changes on the kinetics of the flow and, consequently, on wave-breaking and wave-reflection on the structure, which explains the results at G2. The variability of wave-breaking and wave-reflection explains also this result. Even though, as shown in previous papers (Didier and Neves, 2009b, 2010a), wave propagation is not very dependent on the resolution, while wave breaking is more sensitive to particle dimensions. The same analysis can be made for pressure and force on the vertical wall of the structure. Pressure and force depend greatly on the wave breaking, interaction between incident and reflected waves, and wave impact at the wall. For the finer resolutions, $N = 99222$

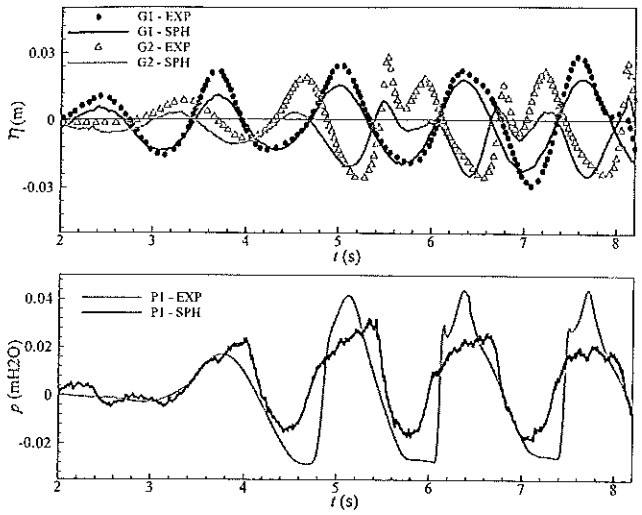

Fig. 7 Free-surface elevation (gauges G1 and G2), pressure (sensor P1) and force on vertical wall ($T = 1.3$ s, $H = 0.04$ m, $d = 0.266$ m)

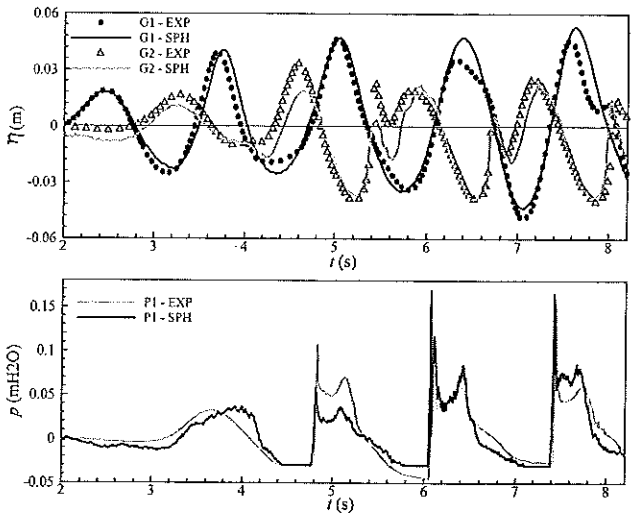

Fig. 9 Free-surface elevation (gauges G1 and G2), pressure (sensor P1) and force on vertical wall ($T = 1.3$ s, $H = 0.08$ m, $d = 0.266$ m)

and 155612, convergence of pressure and force seems to be confirmed, even if some discrepancies appear between the results obtained with these 2 resolutions, specifically for the first and second load pick. Convergence of pressure is very difficult to obtain since some small differences on wave breaking, reflection and/or interaction between the breaking wave and the structure, when resolution is changed, can induce significant changes of pressure at the sensor position and force.

Results of the convergence study indicate that a resolution of at least 36 particles for wave height seems to be required for accurate wave propagation. This result is confirmed hereafter, since the finer resolution of 155612 particles, used in the present numerical simulations, is not enough for smaller wave heights cases.

Figs. 7~13 show the mean time series (i.e. mean of 10 test measurements) of free-surface elevation at gauges G1 and G2 and pressure at sensor P1, for a wave height of 0.04 to 0.16 m, respectively. At sensors P2~P6 less impact occurred, making the results less relevant for the impact analyses of the presented paper. Free-surface elevation and pressure are compared with experimental data. As numerical and physical modeling are performed without dynamic absorption, result analysis is conducted before re-reflection of the wave on the wave-maker reaches the breakwater, which corresponds to 4 wave impacts on the structure.

Good agreement is globally observed between numerical results and experimental data for free-surface elevation, with more significant differences for the smallest (0.04 and 0.06 m) and biggest wave height (0.16 m).

For wave height $H = 0.04$ and 0.06 m, resolution is not enough in term of wave height resolution (15 and 22 particles for each wave height, respectively), confirming the results of the convergence study with resolution which indicate that at least around 36 particles for wave height are necessary for accurate modeling of wave propagation and pressure at the vertical wall of the structure. Numerical results of free-surface elevation, even at gauge G1, are significantly underestimated compared to the experimental data. Another reason for the discrepancies is the imperfection of kinetic energy conservation, particularly for small wave height.

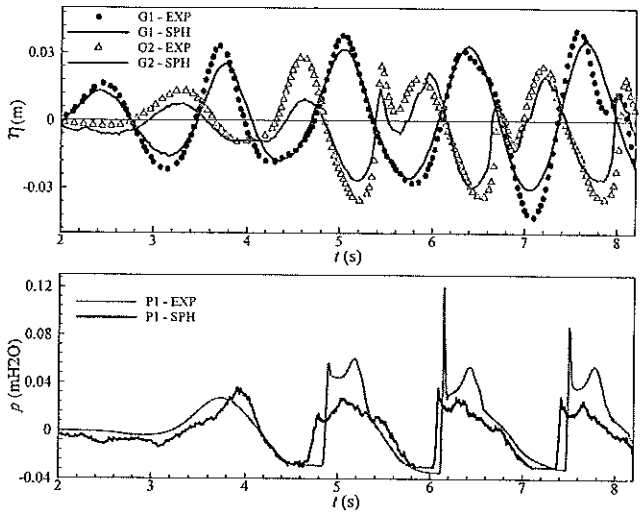

Fig. 8 Free-surface elevation (gauges G1 and G2), pressure (sensor P1) and force on vertical wall ($T = 1.3$ s, $H = 0.06$ m, $d = 0.266$ m)

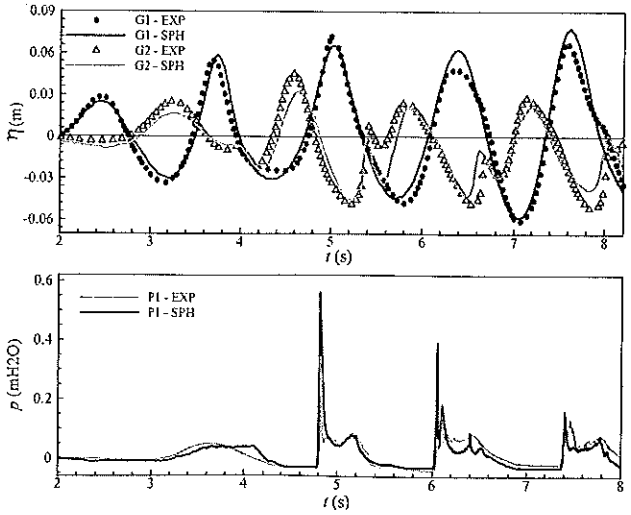

Fig. 10 Free-surface elevation (gauges G1 and G2), pressure (sensor P1) and force on vertical wall ($T = 1.3$ s, $H = 0.10$ m, $d = 0.266$ m)

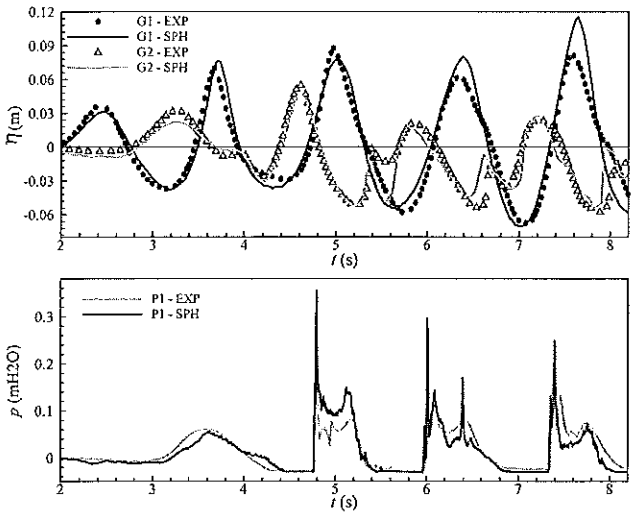

Fig. 11 Free-surface elevation (gauges G1 and G2), pressure (sensor P1) and force on vertical wall ($T = 1.3$ s, $H = 0.12$ m, $d = 0.266$ m)

For wave height $H = 0.16$ m, wave breaking occurs in the vicinity of the wave-maker in the numerical simulation but not during the experimental tests. Superficial tension at the free surface is not included in the numerical model, and it can explain wave instabilities that induce wave breaking.

For the other wave heights tested, between 0.08 m and 0.14 m, agreement between numerical and experimental results is good, and the free-surface elevation pattern is correctly simulated. The resolution is around 30 and 53 particles for wave height 0.08 and 0.14 m, respectively.

Pressure time series obtained numerically exhibit some noise, even with re-normalization of density, and a 1 pass of smoothing is applied using an average mean smoothing on 10 neighboring data points of a value. The pressure variation trend obtained with the numerical model is globally similar to the experimental data for an incident wave height between 0.08 m and 0.16 m. Agreement between numerical and experimental results is good regarding the complexity of the interaction between waves that break and impact on the vertical wall, and the air trapped by breaking

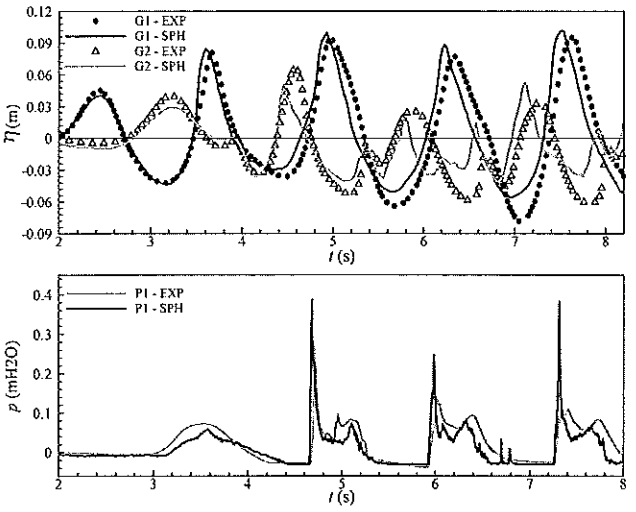

Fig. 12 Free-surface elevation (gauges G1 and G2), pressure (sensor P1) and force on vertical wall ($T = 1.3$ s, $H = 0.14$ m, $d = 0.266$ m)

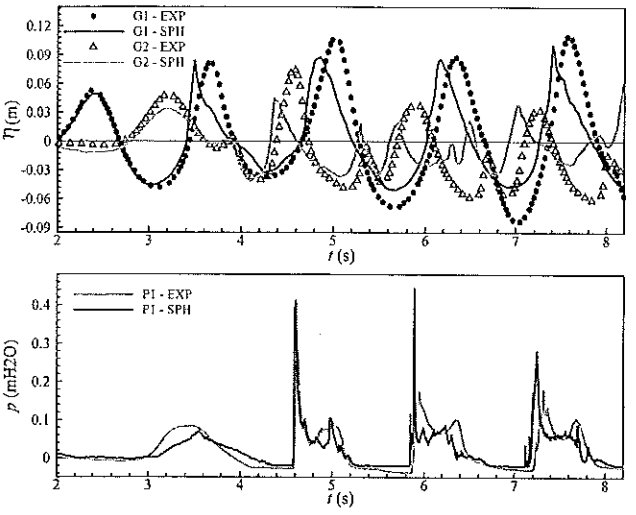

Fig. 13 Free-surface elevation (gauges G1 and G2), pressure (sensor P1) and force on vertical wall ($T = 1.3$ s, $H = 0.16$ m, $d = 0.266$ m)

waves in the physical model which is not taken in account in the code. For smaller wave height, 0.04 and 0.06 m, pressure is not correctly simulated due to the inaccuracy of the wave height near the structure and lack of resolution (noted above).

Fig. 14 shows the horizontal force at the wall for $H = 0.14$ m. Force on the vertical wall of the breakwater is similar to the force trend predicted by the project PROVERBS (1999): a first impact load with a high force value occurs during a short period of time; a second maximum of force occurs due to the collapse of the water column formed at the wall after the first impact, with lower intensity.

Table 2 presents a statistical analysis of the time series of free-surface elevation at G1, G2 and of pressure at P1 for a wave height varying from 0.04 to 0.16 m. *Bias* (mean deviation of numerical results compared to experimental data), *RMS* (root-mean-square) and *IC* (index of agreement) parameter are presented (Willmott et al., 1985).

Bias of sensor P1 is negative, except for $H = 0.04$ m, which indicates that pressure is systematically underestimated for wave height from 0.06 to 0.16 m. *RMS* increases with increase of wave height, as can be expected, and values are around 10% to 30% of mean pressure variation. *IC* is found to be within 80% to 90%, which confirms that the estimation of pressure is relatively good regarding the very complex phenomena occurring during impact loads. It is very difficult for pressure obtained in numerical simulation to agree with pressure measured at a pressure sensor since small differences in the incident wave and/or in the wave-breaking can lead to a different impact point on the vertical breakwater wall, thus leading to large differences on pressure values obtained

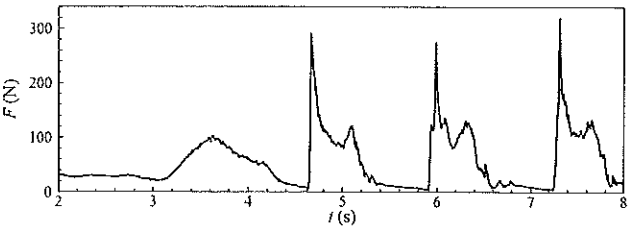

Fig. 14 Time series of horizontal force at vertical wall ($T = 1.3$ s, $H = 0.14$ m, $d = 0.266$m)

H (m)	Gauge/Sensor	*Bias*	*RMS*	*IC*
0.04	G1	−0.00275	0.00549	0.9514
	G2	−0.00448	0.00939	0.7851
	P1	0.00338	0.01255	0.8474
0.06	G1	0.00074	0.00597	0.9754
	G2	−0.00191	0.00803	0.9170
	P1	−0.00580	0.01789	0.8191
0.08	G1	0.00144	0.00669	0.9817
	G2	−0.00349	0.00823	0.9411
	P1	−0.00185	0.01821	0.9049
0.10	G1	0.00180	0.00767	0.9873
	G2	−0.00173	0.00972	0.9432
	P1	−0.00326	0.03615	0.8074
0.12	G1	0.00113	0.01288	0.9762
	G2	−0.00208	0.01149	0.9423
	P1	−0.00202	0.02733	0.8972
0.14	G1	0.00072	0.01967	0.9477
	G2	0.00122	0.02105	0.8114
	P1	−0.00982	0.03710	0.8154
0.16	G1	−0.00043	0.02834	0.8931
	G2	0.00489	0.03032	0.6242
	P1	−0.00081	0.04109	0.8020

Table 2 Statistic values (*Bias*, *RMS* and *IC*) for wave height of 0.04 m to 0.16 m for free-surface elevation at gauges G1 and G2 and for pressure at sensor P1

at numerical and experimental models. Horizontal force on the vertical wall, obtained through the pressure integration, is easier to compare than the pressure at a specific sensor and is the parameter used in structure design.

However, the experimental wave flume was not equipped for measuring force. Details of the maximum pressure occurring during the wave impact are shown in Table 3 and analyzed hereafter.

Bias for free-surface elevation at gauges G1 and G2 shows that the numerical model globally overestimates the free-surface elevation at G1 but underestimates it at G2. At gauge G1, only for wave height 0.04 m and 0.16 m, the free-surface elevation is not overestimated. For gauge G2, the free-surface elevation is slightly underestimated for $H = 0.04$ m to 0.12 m, but overestimated for wave height 0.14 m and 0.16 m. *RMS* tends to increase when wave height increases and to be greater for gauge G2 than for G1. Near the structure, where gauge G2 is located, the free-surface elevation is more variable due to the complexity and variability of the phenomena in this zone where wave breaking, wave reflection and collapse of the water column occur. *IC* for gauge G1 is greater than 94%, except for wave height 0.16 m with $IC = 89\%$. For gauge G2, *IC* is smaller than that obtained for G1 and values are 91%~94%. However, for the smallest wave height, $H = 0.04$ m, *IC* is 78% and for the highest one, $H = 0.14$ and 0.16 m, *IC* is 81% and 62%, respectively. For smaller wave height, the discrepancy is due to lack of resolution (only 15 particles for wave height). For higher waves, large differences are probably due to the complexity of the flow near the structure and of the wave breaking that occurs at the beginning of the flume (for wave height 0.16 m), as noted above. In all the cases, *IC* of gauge G1 is always larger than *IC* of gauge G2. Even though the most interesting parameter to be analyzed is the resultant force, not as susceptible to smaller differences of punctual measurements as occurs with the pressure, one possible solution to enlarge the model accuracy is to refine the resolution.

	Mean error of pressure peak for the first 3 waves	
H (m)	First pressure peak	Second pressure peak
0.08	26.6	24.4
0.10	121.5	42.5
0.12	69.9	58.1
0.14	123.1	15.0
0.16	62.5	16.8

Table 3 Mean error of the first and second pressure peak for the first 3 waves for wave height from 0.08 to 0.16 m

Table 3 shows the relative error between numerical and experimental results regarding the magnitude of the first and second maximum peak pressure that occur during the wave impact. Only the first 3 impacts are considered in this analysis. Error (mean value of the 3 errors between experimental and numerical, for each pressure peak,) is between 26.6% and 123.1% for the first pressure peak and 15.0% and 58.1% for the second, which corresponds to a mean error (mean of the errors obtained for each wave height in Table 3) of 80.7% and 31.4% for the first and second pressure peak, respectively. Numerical estimation of maximum pressure is more accurate for the second pressure peak than for the first. Phenomena involved during the first peak pressure, which corresponds to the impact load, are more complex and variable than those occurring during the second pressure peak, essentially due to the collapse of the water column formed along the vertical wall of the breakwater—even though the global error, regarding the estimation of maximum pressure (first and second peak), is 56.0% with an RMS value of about 38%. Taking into account the phenomena involved, very difficult to be accurately modeled, numerically as well as physically, the differences obtained between physical and numerical results can be considered acceptable, and the numerical model considered to be a suitable tool able to give an order of magnitude of the expected forces at the vertical wall.

Overtopping is observed during the physical model tests for some incident wave heights. However, in numerical simulations, overtopping does not occur. This is probably due to the repulsion boundary type of condition used that tends to repel the particles from the wall.

For the wave period $T = 1.1$ s, the results are very similar to those obtained for $T = 1.3$ s and presented here.

Numerical simulations for water depth 0.325 m have not yet been performed due to the large number of particles necessary to run this case and, consequently, the high CPU.

CONCLUSIONS

The paper presents the validation of the LNEC's version of the SPH numerical model, based on the SPHysics model, for the study of wave interacting with a composite breakwater. To achieve this validation, a set of tests was performed in an LNEC wave flume with the experimental setup and wave generation compatible with the numerical model. Therefore, the flume dimensions are the same for both numerical and physical models and wave generation is identically made using a piston-type wave-maker.

A globally good agreement is found between numerical results and experimental data regarding free-surface elevation at 2 gauges, G1 and G2, and pressure at a sensor P1 for an incident wave with a 1.3 s period, wave height from 0.04 m to 0.16 m, and a water depth of 0.266 m. A convergence study with resolution, i.e. particle dimension, for $H = 0.12$ m, shows that a resolution of

at least 36 particles for wave height is required for accurate propagation of the wave and estimation of the pressure at the vertical breakwater wall. Comparing numerical and experimental results for $H = 0.04$ m to 0.16 m, with a fine resolution of 155612 particles (particle dimension equal to 2.66 mm), it appears that the accuracy of the numerical model is obtained for around 30 particles for wave heights, since for smaller wave heights, 0.04 m and 0.06 m (resolution of 15 and 22 particles for wave height, respectively) numerical results are strongly underestimated. For wave heights from 0.08 m to 0.14 m, 30 to 53 particles for wave height, respectively, a good agreement between numerical results and experimental data is obtained.

It was shown that the force behavior on the vertical wall of the breakwater is similar to the forecast by the project PROVERBS for impact load, with a first impact with a high force intensity during a very short time, and a second maximum of pressure, due to the collapse of the water column formed at the wall after the first impact, smaller than the first.

Statistical analysis shows that pressure is globally underestimated, RMS values are 10% to 30% of mean pressure variation, and *IC* value is 80% to 90%. Error on the 2 peaks of pressure is between 26.6% and 123.1% for the first peak and 15.0% and 58.1% for the second, which corresponds to a mean error (for all wave heights) of 80.7% and 31.4% for the first and second peaks of pressure, respectively. The global error, regarding the estimation of the maximum of pressure (first and second peaks), is 56.0% with an RMS value of about 38%. These results depend highly on wave breaking and the difficulty of capturing the high-pressure peaks and may explain the errors obtained. Nevertheless, the evolution in time of the forces and pressure is well modeled.

The numerical model, globally, overestimates slightly the free-surface elevation in the middle of the flume (G1) but underestimates near the breakwater (G2), which is believed to be caused by the density renormalization of fluid particles near the structure, as well as the stochastic nature of the flow (wave breaking and wave reflection) close to the breakwater. In all the cases, *IC* of G1 is always larger than *IC* of G2. *IC* for gauge G1 is greater than 94% and is slightly smaller for gauge G2 with values of 91%~94%. For the smallest wave height, $H = 0.04$ m, and for the largest ones, $H = 0.14$ m and 0.16 m, *IC* is less than 90%.

ACKNOWLEDGEMENTS

Eric Didier acknowledges the financial support given by the Portuguese Science and Technology Foundation, SFRH/BPD/37901/2007. The authors acknowledge the financial support given by the Portuguese Science and Technology Foundation for the Project SPACE—PTDC/ECM/114109/2009.

REFERENCES

Batchelor, GK (1974). *Introduction to Fluid Dynamics*, Cambridge Univ Press, UK.

Colagrossi, A, and Landrini, M (2003). "Numerical Simulation of Interfacial Flows by Smoothed Particle Hydrodynamics," *J Comp Phys*, Vol 191, pp 448–475.

Crespo, AJC, Gómez-Gesteira, M, and Dalrymple, RA (2008a). "Modeling Dam Break Behavior over a Wet Bed by a SPH Technique," *J Waterways, Port, Coastal, and Ocean Eng*, Vol 134, No 6, pp 313–320.

Crespo, AJC, Gómez-Gesteira, M, Narayanaswmy, MS, and Dalrymple, RA (2008b). "A Hybrid Boussinesq-SPH Model for Coastal Wave Propagation," *Proc 3rd ERCOFTAC SPHERIC Wksp*, Lausanne, Switzerland, pp 11–16.

Dalrymple, RA, Knio, O, Cox, DT, Gomez-Gesteira, M, and Zou, S (2001). "Using Lagrangian Particle Method for Deck Overtopping," *Proc MOF the Waves, ASCE*, pp 1082–1091.

Dalrymple, RA, and Rogers, BD (2006). "Numerical Modeling of Water Waves with the SPH Method," *Coastal Eng*, Vol 53, Nos 2–3, pp 141–147.

Didier, E, and Neves, MG (2009a). "Wave Overtopping of a Typical Coastal Structure of the Portuguese Coast Using a SPH Model," *J Coastal Res*, SI 56, pp 496–500.

Didier, E, and Neves, MG (2009b). "Coastal Flow Simulation Using SPH: Wave Overtopping on an Impermeable Coastal Structure," *Proc 4th ERCOFTAC SPHERIC Wksp*, pp 357–364, Nantes, France.

Didier, E, and Neves, MG (2010a). "A Lagrangian Smoothed Particles Hydrodynamics–SPH– Method for Modelling Waves-Coastal Structure Interaction," *Proc CFD2010 ECCOMAS*, Lisbon.

Didier, E, and Neves, MG (2010b). "Study of Wave Interaction with Coastal Structures Using a SPH Numerical Model," *J Integrated Coastal Zone Management*, Vol 10, No 4, pp 435–455.

Didier, E, Martins, R, Neves, MG, and Vasco, JRG (2011). "Interaction Between Wave and Coastal Structure: Validation of Two Lagrangian Numerical Models with Experimental Results," *Proc MARINE 2011 Computat Meth in Marine Eng IV*, pp 134–145, Lisbon.

Didier, E, and Neves, MG (2012). "A Semi-Infinite Numerical Wave Flume Using Smoothed Particle Hydrodynamics," *Int J Offshore and Polar Eng*, ISOPE, Vol 22, No 3, pp 193–199.

Gómez-Gesteira, M, Rogers, BD, Dalrymple, RA, Crespo, AJC, and Narayanaswamy, M (2008). "User Guide for the SPHysics Code v1.4," http://wiki.manchester.ac.uk/sphysics.

Gómez-Gesteira, M, Rogers, BD, Dalrymple, RA, and Crespo, AJC (2010). "State-of-the-Art of Classical SPH for Free-Surface Flows," *J Hydraulic Res*, Vol 48 Extra Issue, pp 6–27.

Gotoh, H, Shibahara, T, and Sakai, T (2001). "Sub-Particle-Scale Turbulence Model for the MPS Method – Lagrangian Flow Model for Hydraulic Engineering," *Computat Fluid Dyn J*, Vol 9, No 4, pp 339–347.

Hughes, JP, and Graham, DI (2010). "Comparison of Incompressible and Weakly-Compressible SPH Models for Free-Surface Water Flows," *J Hydraulic Res*, Vol 48 Extra Issue, pp 105–117.

Johnson, G, Stryk, R, and Beissel, S (1996). "SPH for High Velocity Impact Calculations," *Comp Methods in Appl Mech and Eng*, Vol 139, pp 347–373.

Martins, R (2012). "Analysis of Interaction Between Regular Wave and Vertical Breakwater Using a Smoothed Particle Hydrodynamics Numerical Model," *Master's Thesis*, Universidade Nova de Lisboa (in Portuguese).

Monaghan, JJ (1989). "On the Problem of Penetration in Particle Methods," *J Computat Phys*, Vol 82, pp 1–15.

Monaghan, JJ (1992). "Smoothed Particle Hydrodynamics," *Ann Rev Astro and Astrophys*, Vol 30, pp 543–574.

Monaghan, JJ (1994). "Simulating Free Surface Flows with SPH," *J Computat Phys*, Vol 110, pp 399–406.

Monaghan, JJ, and Kos, A (1999). "Solitary Waves on a Cretan Beach," *J Waterways, Ports, Coastal and Ocean Eng*, Vol 125, pp 145–154.

PROVERBS (1999). http://www.tu-bs.de/~i5102401.

Rogers, BD, and Dalrymple, RA (2004). "SPH Modeling of Breaking Waves," *29th Int Conf Coastal Eng*, World Scientific Press, pp 415–427.

Rogers, BD, Dalrymple, RA, and Stansby, PK (2010). "Simulation of Caisson Breakwater Movement Using 2-D SPH," *J Hydraulic Res*, Vol 48 Extra Issue, pp 135–141.

Shao, S (2010). "Incompressible SPH Flow Model for Wave Interactions with Porous Media," *Coastal Eng*, Vol 57, pp 304–316.

SPHysics code, version 1.4 (2008), http://wiki.manchester.ac.uk/sphysics.

Willmott, CJ, Ackleson, SG, Davis, RE, Feddema, JJ, Klink, KM, Legates, DR, O'Donnell, J, and Rowe, CM (1985). "Statistics for the Evaluation and Comparison of Models," *J Geophys Res*, Vol 90(c5), pp 8995–9005.

The Proceedings of
The Twenty-second (2012) International
OFFSHORE AND POLAR ENGINEERING CONFERENCE
Rhodes, Greece, June 17–22, 2012

ISBN 978–1–880653–94–4 ISSN 1098–6189
Indexed by Engineering Index, Compendex, and others.

VOLUME I

FRONTIER ENERGY, GAS HYDRATES & OCEAN MINING
Clean Energy and Clean Coal, Gas Hydrate Fundamentals, Gas Hydrate Development, Gas Hydrate Modeling, Deep Ocean Mining
RENEWABLE ENERGY (WIND AND OCEAN)
Wind Turbine Foundation and Structure, Offshore Wind Energy – Floating Systems, Dynamics and Analysis, Concepts, Codes and Design, Offshore Wind Energy Resources and Power, Wave Energy Resources, Wave Energy and Systems, Tidal and Ocean Current Energy, Ocean Thermal Energy Conversion
ENVIRONMENT SCIENCE AND ENGINEERING
Oil Pollution and Water Quality, Physical and Chemical Processes, Water and Sediment Qualities
OFFSHORE MECHANICS AND HYDRODYNAMICS
Floating Storage and Regasification Unit (FSRU), FPSO and LNG Transport, Floating Dynamics, Ocean Systems, Deepwater Design and Installation, Moored Structures,
ARCTIC SCIENCE AND TECHNOLOGY
Navigation in Pack Ice, Ice Mechanics, Coastal Arctic Properties, Ice Environment and Forecasting, Ice–Structure Interactions, Operations in Ice, Operations in Ice, Ice Modeling and Operations

VOLUME II

PLENARY PRESENTATIONS
Pipeline Qualification for PNG LNG Project, From the Longest to the Deepest Pipelines
OFFSHORE PIPELINES, RISERS AND MOORING
NORD Stream, New Concept Development, System Integrity, Component Development, Installation and Fabrication, Installation and Fabrication, Fatigue Assessment, Advanced Analysis, Internal and External Flow Effects, Improved Systems Performance
UNDERSEA VEHICLE, COMMUNICATION AND CONTROL
Underwater Acoustics, Monitoring and Communication, Underwater Vehicle, Robotics and Control
GEOTECHNICAL AND GEOENVIRONMENTAL ENGINEERING
Soil Properties, Soil Improvement, Suction Piles, Offshore Foundations, Piles and Foundations, Cyclic Loading, Slope Stability, Consolidation and Seepage, Materials and Test

VOLUME III

HYDRODYNAMICS
TSUNAMI AND SAFETY
2011 Tohoku Tsunami, Tsunami Generation and Warning; Tsunami Propagation and Flooding, Tsunami Effect on Structure and Sediment, Tsunami Risk Assessment
SLOSHING DYNAMICS AND DESIGN
Progress at GTT, Physics and Coupling, LNG Tank Design, Sloshing Tests, CFD in Sloshing, Structural Responses to Sloshing
FLOW-INDUCED VIBRATIONS
HYDRODYNAMICS
CFD, MetOcean, Freak Waves and Long Waves, Wave Loading, Floating-Body Dynamics, Dynamic Positioning and Control,
COASTAL ENGINEERING
Waves and Modeling, Breakwaters and Waves, Wave-Structure Interactions, Estuary Hydraulics, Coastal Sediment, Storm Surge and Inundation

VOLUME IV

HIGH-PERFORMANCE MATERIALS (HPM)
Advanced Materials and Structures, Shipbuilding Steels, Composites, Fatigue and Fracture, Advances in Welding Technology,
ARCTIC MATERIALS
Materials and Development, Steel and Weldment, Weldment and Coatings
ASSET INTEGRITY
STRAIN-BASED DESIGN
Materials , , Numerical Modeling , Strain Capacity Characterization, Fracture Mechanics
RISK AND RELIABILITY
Risk and Reliability, Risk and Fatigue
ADVANCED SHIP TECHNOLOGY
At-Sea Explosions, Collision and Vibration, Slamming and Load, Ultimate Strength, Seakeeping and Resistance, Propulsion, System Design